Electronic and vibrational spectroscopy of intermediates in methane-to-methanol conversion by CoO^+

Gokhan Altinay, Abdulkadir Kocak, Jennifer Silva Daluz, and Ricardo B. Metz[a)]
Department of Chemistry, University of Massachusetts Amherst, Amherst, Massachusetts 01003, USA

(Received 10 May 2011; accepted 28 July 2011; published online 26 August 2011)

At room temperature, cobalt oxide cations directly convert methane to methanol with high selectivity but very low efficiency. Two potential intermediates of this reaction, the $[HO–Co–CH_3]^+$ insertion intermediate and $[H_2O–Co{=}CH_2]^+$ aquo-carbene complex are produced in a laser ablation source and characterized by electronic and vibrational spectroscopy. Reaction of laser-ablated cobalt cations with different organic precursors seeded in a carrier gas produces the intermediates, which subsequently expand into vacuum and cool. Ions are extracted into a time-of-flight mass spectrometer and spectra are measured via photofragment spectroscopy. Photodissociation of $[HO–Co–CH_3]^+$ in the visible and via infrared multiple photon dissociation (IRMPD) makes only $Co^+ + CH_3OH$, while photodissociation of $[H_2O–Co{=}CH_2]^+$ produces $CoCH_2^+ + H_2O$. The electronic spectrum of $[HO–Co–CH_3]^+$ shows progressions in the excited state Co–C stretch (335 cm^{-1}) and O–Co–C bend (90 cm^{-1}); the IRMPD spectrum gives $\nu_{OH} = 3630\ cm^{-1}$. The $[HO–Co–CH_3]^+(Ar)$ complex has been synthesized and its vibrational spectrum measured in the O–H stretching region. The resulting spectrum is sharper than that obtained via IRMPD and gives $\nu_{OH} = 3642\ cm^{-1}$. Also, an improved potential energy surface for the reaction of CoO^+ with methane has been developed using single point energies calculated by the CBS-QB3 method for reactants, intermediates, transition states and products. © *2011 American Institute of Physics*. [doi:10.1063/1.3626412]

I. INTRODUCTION

The direct and efficient conversion of methane to methanol,

$$CH_4 + 1/2\,O_2 \rightarrow CH_3OH, \quad (1)$$

has long been a "holy grail" of catalysis.[1] In nature, direct methane-methanol conversion is catalyzed by methane monooxygenases (MMOs). Soluble MMO contains an iron-oxo center;[2] particulate MMO has copper at the active site. In the laboratory, this "holy grail" has yet to be realized, as reaction efficiencies are low. For example, direct oxidation of methane by a H_2/O_2 mixture using a $FePO_4$ catalyst shows 80% selectivity for methanol production at 630 K, but the rate of methane conversion is very low, 0.02 μmol m^{-2} s^{-1}; higher temperatures improve the conversion rate, but the selectivity decreases.[3] There has been considerable progress in direct methane-methanol conversion using metal-doped zeolites. Although most of these systems require N_2O as the oxidant, Bitter and co-workers report production of 1.2 μmol methanol/g catalyst with ~75% selectivity with O_2 as the oxidant using cobalt-doped ZSM-5 zeolites.[4] Unfortunately, this is not a continuous process, but rather involves calcining the zeolite in air at 550 °C, reaction with methane at 150 °C, and extraction of the product using ethanol. Other promising results include direct oxidation of methane to a methyl ester using a platinum catalyst[5] and the synthetically useful oxidation of unactivated C–H bonds using an iron-based catalyst with H_2O_2 as the oxidant.[6]

In 1990, Schröder and Schwarz observed that gas-phase FeO^+ reacts efficiently with methane at room temperature, producing methanol with good selectivity.[7] As a result, the reactions of gas-phase metal oxide cations with methane have been systematically investigated, at room temperature using ion cyclotron resonance (ICR) spectrometers and selected ion flow tubes, and at hyperthermal energies using guided ion beams. The first-row transition metal oxides have been most extensively studied. Their room-temperature reaction efficiencies and selectivities vary greatly. The early metals ScO^+, TiO^+, VO^+, and CrO^+ exhibit no reactivity toward methane, due to their strong metal-oxygen bonds. Although MnO^+ reacts with methane very efficiently, $MnOH^+ + CH_3$ is the major product; the branching ratio to methanol is less than 1%.[8] FeO^+ reacts efficiently, forming methanol with 41% selectivity (the major product is $FeOH^+ + CH_3$).[7,9] CoO^+ reacts very inefficiently, at only 0.5% of the collision rate, but the branching ratio to methanol is 100%.[10,11] NiO^+ exhibits efficient reactivity and high methanol branching ratio,[12,13] and it was recently determined that CuO^+ also reacts efficiently with CH_4, producing methanol with 60% selectivity (the other major product is $CuOH^+ + CH_3$).[14]

Reactions of gas-phase transition metal oxide cations MO^+ with methane are thus a simple model system for the direct conversion of methane to methanol, which has spurred extensive experimental and computational studies.[9,12,13,15–18] The key intermediates in the reaction are the $OM^+(CH_4)$ entrance channel complex, $[HO–M–CH_3]^+$ insertion intermediate and $M^+(CH_3OH)$ exit channel complex.

The reverse reaction – reaction of Co^+ and its cluster ions with methanol – has also been investigated. Allison

a)Electronic mail: rbmetz@chem.umass.edu.

and Ridge studied reactions of several metal cations with methanol in an ICR spectrometer. They observed no reaction with Co^+. Reaction of $Co^+(CO)$ with methanol leads to ligand exchange, producing $[CoCH_4O]^+$.[19] As part of a detailed study of methane-to-methanol conversion by CoO^+, Chen *et al.* studied the reaction of Co^+ with CH_3OD as a function of collision energy.[11] The lowest energy product is $CoOD^+$, which has an onset near 0.8 eV collision energy, and dominates until ~4 eV collision energy, where $CoCH_3^+$, CoH^+, and CH_2OD^+ also become competitive. Oiestad and Uggerud investigated the reaction of cobalt cluster ions Co_n^+ (n = 1–12) with methanol. Atomic Co^+ reacts very inefficiently and forms a $[CoCH_4O]^+$ adduct. Adduct formation is much more efficient with larger Co_n^+ clusters (n = 2–5). These clusters also dehydrogenate methanol.[20] Hirabayashi *et al.* measured spectra of methanol adsorbed onto cobalt cluster ions $Co_n^+(CH_3OH)_m$ (n = 2–6, m = 1–3) in the O–H and C–H stretching region.[21] For the smallest system studied, $Co_2^+(CH_3OH)$ they observe very inefficient infrared multiple photon dissociation (IRMPD), and the O–H stretch $\nu_{OH} = 3624\ cm^{-1}$. Clusters with more cobalt atoms have slightly higher values $\nu_{OH} \approx 3638\ cm^{-1}$, closer to the value in bare methanol ($\nu_{OH} = 3681\ cm^{-1}$).[22] Inserted complexes $Co_n^+(CH_3)(OH)$ may also contribute to the spectra.

Our group has studied the electronic spectroscopy of intermediates of the $FeO^+ + CH_4$ reaction in the visible and near-UV region. By using specific ion-molecule reactions, two intermediates ($[HO–Fe–CH_3]^+$ and $[H_2O–Fe{=}CH_2]^+$) of the $FeO^+ + CH_4$ reaction were prepared and their electronic spectra examined. The photodissociation spectrum has well-resolved vibrational structure, with progressions in the Fe–C stretch, Fe–O stretch and O–Fe–C bend.[23]

We recently measured vibrational spectra of the $[HO–Fe–CH_3]^+$ insertion intermediate and $Fe^+(CH_3OH)$ exit channel complex of methane to methanol conversion by FeO^+.[24] Vibrational spectra of these intermediates in the O–H and C–H stretching regions were measured by IRMPD and by monitoring argon atom loss following irradiation of $Fe^+(CH_3OH)(Ar)$ and $[HO–Fe–CH_3]^+(Ar)_n$ (n = 1, 2). FeO^+ and CoO^+ exhibit very different reaction efficiencies and selectivities for methane activation, which motivates this study. Photofragmentation of $[HO–Fe–CH_3]^+$ in the near-UV produces similar quantities of Fe^+ (and methanol) and $FeOH^+$ (and CH_3), which mirrors the products observed in the bimolecular reaction. Thus, it will be interesting to determine the photodissociation pathways of $[HO–Co–CH_3]^+$.

II. EXPERIMENTAL AND THEORETICAL METHODS

Electronic and vibrational spectra are measured using a dual time-of-flight reflectron photofragment spectrometer.[16,25] Cobalt cations are generated by laser ablation of a cobalt rod (Sigma-Aldrich, 99.8% pure) and then react with a suitable organic precursor diluted in a carrier gas (He, Ar, or a mixture) to produce the target molecule. The choice of precursors is guided by those used by Chen *et al.*[11] in guided ion beam studies of $CoO^+ + CH_4$ reaction intermediates and in the collisional activation studies of Schröder *et al.*[26] and our spectroscopic studies of intermediates of the $FeO^+ + CH_4$ reaction.[23,24] Details of the precursors used and characterization of the intermediates produced are discussed in Sec. III B. Ions produced in the source expand supersonically into vacuum and cool to a rotational temperature of ~10 K.[27] Ions are accelerated to 1800 V kinetic energy, then re-referenced to ground potential before entering the field-free flight tube. Mass-selected ions are photodissociated at the turning point of the reflectron.

Energetically, photodissociation of $[HO–Co–CH_3]^+$ requires at least three photons in the O–H stretching region. So, vibrational spectra are obtained using IRMPD of $[HO–Co–CH_3]^+$, $[H_2O–Co{=}CH_2]^+$ and, perhaps, $Co^+(CH_3OH)$, and IR resonance-enhanced photodissociation (IR-REPD) of argon tagged molecules $[HO–Co–CH_3]^+(Ar)$. The photodissociation efficiency is greatly improved by using a multi-pass mirror arrangement[28] in which the laser makes 21 passes through the ion cloud. The IR light source is a Nd:YAG-pumped optical parametric oscillator which is tunable from 2 to 5 μm, producing ~10 mJ/pulse near 3600 cm^{-1}. The IR beam path is purged with nitrogen to minimize absorptions by atmospheric water vapor. The laser wavelength is calibrated using H_2O and CH_4 absorptions. For the electronic spectroscopy, the light source is a Nd:YAG-pumped tunable dye laser. Fragment ions and undissociated parent ions are detected by a dual micro-channel plate detector. The ion signal is amplified, collected on a digital oscilloscope or a gated integrator, and averaged with a LABVIEW-based program. The photodissociation spectrum is obtained by monitoring the yield of the fragment ion of interest as a function of wavelength and normalizing to parent ion signal and laser fluence. The photodissociation spectrum is the product of the absorption spectrum and the photodissociation quantum yield.

Computations are carried out with the GAUSSIAN 2003 program package.[29] Optimized geometries of the reactants, intermediates, transition states and products are calculated using the Becke Lee-Yang-Parr hybrid HF/density functional theory (DFT) method (B3LYP) with the 6-311+G(*d*,*p*) basis set. Vibrational frequencies are computed to ensure that all optimized geometries correspond to a local minimum or a first-order saddle point (for transition states). Vibrational frequencies are scaled by 0.961, as recommended for this method and basis set by Andersson and Uvdal.[30] More accurate energies are calculated using the complete basis set (CBS-QB3) procedure.[31]

III. RESULTS AND DISCUSSION

This section is organized as follows. First, the calculated potential energy surface (PES) and mechanism of the $CoO^+ + CH_4$ reaction will be presented. Then, precursors and source conditions used to generate specific reaction intermediates and their identification will be discussed. Finally, electronic and vibrational spectroscopy will be used to characterize the intermediates.

A. Mechanism of the $CoO^+ + CH_4$ reaction

To establish the accuracy of the computational methods used, we compare calculated and accurate experimental

TABLE I. Experimental and calculated (CBS-QB3) values of thermodynamic quantities related to the $CoO^+ + CH_4 \rightarrow Co^+ + CH_3OH$ reaction. All values are in kJ/mol, at 0 K. The experimental ΔH_{rxn} are based on $D_0(Co^+–O)$ and $D_0(Co^+–OH)$,[11,40] and ΔH_f^0 of O, CH_4, and CH_3OH.

	CBS-QB3	Expt.
$D_0(Co^+–O)$	291	314 ± 4 (Ref. 40)
$D_0(Co^+–CH_3OH)$	181	148 ± 8 (Ref. 11)
ΔH_{rxn} $CoO^+ + CH_4 \rightarrow Co^+ + CH_3OH$	−82	−58 ± 5
ΔH_{rxn} $CoO^+ + CH_4 \rightarrow CoOH^+ + CH_3$	11	23 ± 10
Co^+ ^3F–^5F splitting	63	41.4
$D_0(Co^+–OH)$	289	300 ± 4 (Ref. 40)
$D_0(Co^+–H_2O)$	155	161 ± 6 (Ref. 40)
$D_0(Co^+–CH_2)$	308	318 ± 5 (Ref. 40)
$D_0(Co^+–CH_3)$	198	203 ± 4 (Ref. 40)

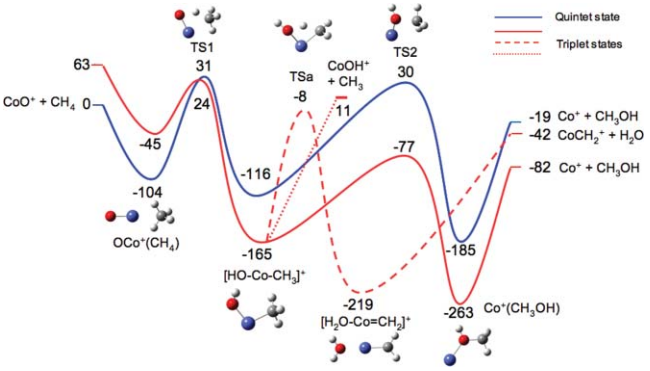

FIG. 1. Schematic potential energy surface for the $CoO^+ + CH_4$ reaction and structures of intermediates and transition states. Energies (in kJ/mol) are calculated at the CBS-QB3 level of theory. The blue line represents the quintet and the red lines represent the triplet surfaces.

results for the tripet-quintet energy splitting in Co^+, the Co^+–O bond enthalpy, and the overall exothermicity of the $CoO^+ + CH_4 \rightarrow Co^+ + CH_3OH$ reaction (Table I). Experimentally, the ground state of Co^+ is ^3F ($3d^8$), with the ^5F ($3d^7$ $4s^1$) state 41.4 kJ/mol higher (this is the weighted average of the spin-orbit levels).[32] Density functional methods give a wide range of values for the triplet-quintet splitting, depending on the basis set. The difficulties in devising basis sets that treat the 3*d* and 4*s* orbitals in a balanced manner is a longstanding problem in density functional-based methods.[33] Calculations at the B3LYP level by Yoshizawa *et al.* using a partially uncontracted, augmented Wachters basis set incorrectly predict a quintet ground state, 35 kJ/mol below the triplet state.[18] On the other hand, B3LYP calculations with the TZVP basis set give the correct ordering, with the triplet 70 kJ/mol below the quintet.[34]

A more reliable[35] alternative to density functional-based calculations are hybrid methods developed for accurate thermochemistry, such as the CBS-QB3 approach.[31] The CBS-QB3 method has been used to characterize the PES for the $FeO^+ + CH_4$ and $CuO^+ + CH_4$ reactions.[14,24] The CBS-QB3 procedure starts with optimizing the geometry and calculating harmonic frequencies at the B3LYP level. Then, from a series of single point energy calculations at various levels of theory and with different basis sets, one extrapolates the result of a large basis set calculation at a very high level of theory. Energies calculated using CBS-QB3 have similar accuracy to an extrapolated series of coupled-cluster single double (triple) (CCSD(T)) calculations with very large basis sets, and are significantly more accurate than a single CCSD(T) calculation with a modest basis set.[36] CBS-QB3 calculations correctly predict the ordering of the Co^+ states, with the quintet 63 kJ/mol above the triplet. The CBS-QB3 calculations slightly underestimate the Co^+–O bond enthalpy. As a result, they slightly overestimate the exothermicity of the $CoO^+ + CH_4$ reaction. The calculations predict that the $Co^+(CH_3OH)$ exit channel complex is bound by 181 kJ/mol relative to $Co^+ + CH_3OH$, which is slightly higher than the experimental value[11] of 148 ± 8 kJ/mol. Overall, for the quantities shown in Table I, CBS-QB3 values are in good agreement with experiment, with a mean absolute deviation of 16 kJ/mol.

Figure 1 shows the potential energy surface for the $CoO^+ + CH_4$ reaction calculated using the CBS-QB3 method. Methanol production occurs in a two-step concerted manner through the formation of the hydroxy intermediate $[HO–Co–CH_3]^+$. The minimum energy path involves first producing the $OCo^+(CH_4)$ entrance channel complex. Hydrogen abstraction via TS1 leads to the key $[HO–Co–CH_3]^+$ insertion intermediate. The CoO^+ reactant has a quintet ground state.[37] Triplet and quintet TS1 have similar energies, and both lie above ground state reactants. The overall reaction *efficiency* is determined by the probability that reactants will cross TS1. This can occur via quintet TS1 or over the slightly lower triplet TS1 following a spin change. Since both TS1 lie ~25 kJ/mol above the reactants, it is not surprising that the efficiency for the thermal reaction is only 0.5%.[10,12]

The calculations predict that, from $[HO–Co–CH_3]^+$ through to products, the minimum energy pathway is clearly the triplet. Figure 2 shows the structures of the triplet intermediates calculated at the B3LYP/6-311+G(*d*,*p*) level. $[HO–Co–CH_3]^+$ is quite bent, with a O–Co–C angle of 104°, a Co–C bond length of 1.93 Å and a Co–O bond length of 1.71 Å. Once produced, the $[HO–Co–CH_3]^+$ insertion intermediate can dissociate to $CoOH^+ + CH_3$ or isomerize via TS2 to form the $Co^+(CH_3OH)$ exit channel complex, which subsequently dissociates to $Co^+ + CH_3OH$. In $Co^+(CH_3OH)$ the Co–O bond length is 1.95 Å. The *selectivity* to produce methanol rather than methyl radical is primarily determined by the relative energies of TS2 and methyl radical products. Methyl radical is produced by simple bond fission, so it is entropically favored over methanol production, which occurs via the tight transition state TS2. If TS2 is at an energy close to or above methyl radical products, then $MOH^+ + CH_3$ products dominate, as is observed for MnO^+.[12,17] For the $FeO^+ + CH_4$ reaction, CBS-QB3 calculations[24] predict that TS2 lies 39 kJ/mol below $FeOH^+ + CH_3$. Under thermal conditions, methyl radical production is slightly favored over methanol, and the methyl radical channel becomes increasingly favorable at higher collision energy.[9] For the $CoO^+ + CH_4$ reaction, triplet TS2 lies 88 kJ/mol below $CoOH^+ + CH_3$. As a result, the thermal reaction is 100% selective for $Co^+ + CH_3OH$ production.[10] However, higher translational energy strongly favors methyl radical formation.[11]

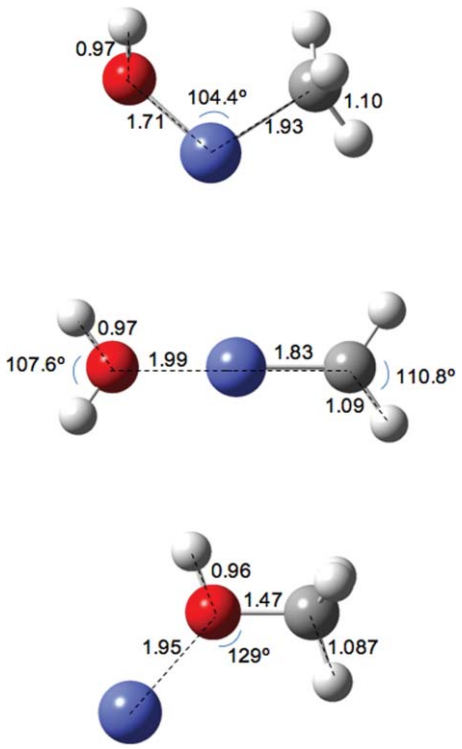

FIG. 2. Calculated structures of triplet intermediates: $[HO–Co–CH_3]^+$ (top), $[H_2O–Co=CH_2]^+$ (middle), and $Co^+(CH_3OH)$ (bottom) calculated at the B3LYP/6-311+G(*d,p*) level.

Reaction of *excited* CoO^+ with methane also produces $CoOH^+ + CH_3$.[10]

The $[HO–Co–CH_3]^+$ insertion intermediate can also isomerize via TSa to form the aquo-carbene intermediate $[H_2O–Co=CH_2]^+$, which then produces $CoCH_2^+ + H_2O$.[38] This product is not observed in the bimolecular reaction, as TSa and TS2 are similarly tight transition states, but TS2 is calculated to lie 69 kJ/mol lower in energy. TSa is a four-center transition state, with Co–O and Co–C bond lengths of 1.887 Å and 2.065 Å, respectively, and a O–Co–C angle of 80°. The reaction coordinate is a hydrogen transfer, with O–H and C–H distances of 1.264 Å and 1.399 Å at the transition state, respectively. The aquo-carbene intermediate has a short 1.83 Å Co–C bond, and a 1.99 Å Co–O distance. Production of the metal carbene and water is the major pathway (70%) in the reaction of PtO^+ with methane, with methanol production accounting for the remaining 30%.[39] For the PtO^+ reaction, TSa is calculated to lie 2 kJ/mol below TS2 at the PCI-80 level, due to the very strong Pt=C bond.[39]

Our CBS-QB3 results are in good agreement with guided ion beam mass spectrometry experiments of Chen *et al.*[11] They find that the $CoO^+ + CH_4 \rightarrow Co^+ + CH_3OH$ reaction has an onset of 54 ± 8 kJ/mol. Overall, the reaction is exothermic, so they associate this onset with the reaction barrier TS1 (Fig. 1). The experiments could not determine the multiplicity of the transition state accessed. Our calculations predict slightly lower reaction barriers of 24 kJ/mol for the triplet state and 31 kJ/mol for the quintet. The measured onset could correspond to either the quintet barrier, or to the triplet barrier, if quintet-triplet conversion is efficient. The calculations predict such similar barriers for the two spin states that we cannot distinguish between the two possibilities. However, it is clear from the experiments that at low energies the reaction to produce $Co^+ + CH_3OH$ proceeds via the triplet TS2, as this lies significantly below quintet TS2. Quintet TS2 lies above the energy of $CoOH^+ + CH_3$, so the methyl radical product would dominate at low energies if the reaction remained on the quintet surface. The potential energy surface in Figure 1 is similar to previous B3LYP results of Yoshizawa and co-workers.[17,18] The most significant difference is that the specific basis set used for cobalt in their B3LYP calculations incorrectly predicts that triplet Co^+ lies 35 kJ/mol above quintet Co^+, leading to significant error in the exothermicity of the overall reaction. In addition, the relative energies of the triplet and quintet insertion intermediates and TS2 are ~40 kJ/mol lower than our computed results.

B. Synthesis and characterization of $[HO–Co–CH_3]^+$, $[H_2O–Co=CH_2]^+$, and $Co^+(CH_3OH)$

A major challenge in these studies is to find suitable precursors and reaction conditions to selectively produce specific intermediates. Our choice of precursors is guided by our previous studies of the electronic[23] and vibrational[24] spectroscopy of intermediates of the $FeO^+ + CH_4$ reaction, by collisional activation studies[26] of $[FeCH_4O]^+$, and by precursors used in guided ion beam studies of $CoO^+ + CH_4$ intermediates.[11] The intermediates formed are characterized by their vibrational and electronic photodissociation spectra, and by the observed photofragments. In this work, we find that reaction of Co^+ with different precursors – methanol, acetic acid, n-propanol – produces $[HO–Co–CH_3]^+$, $[H_2O–Co=CH_2]^+$, and $Co^+(CH_3OH)$, with the relative amounts depending on the precursor.

In the guided ion beam experiments of Chen *et al.*, $Co^+(CH_3OH)$ is made in the flow tube source by reacting Co^+ with *methanol* in 0.65 Torr He/0.06 Torr Ar.[11] Schröder *et al.* react Fe^+ with several precursors in a chemical ionization source and characterize the $[FeCH_4O]^+$ ions formed based on their fragmentation patterns following collisional activation (CA).[26] They find that reaction of Fe^+ with CH_3OH produces the $Fe^+(CH_3OH)$ exit channel complex. In our source, reaction of laser-ablated Fe^+ with methanol seeded in helium or argon produces a mixture of $Fe^+(CH_3OH)$ and $[HO–Fe–CH_3]^+$, with the relative amounts depending on the carrier gas and the ablation laser – pulsed valve delay. Here, we find a similar result: reacting methanol with laser-ablated Co^+ produces both $Co^+(CH_3OH)$ and $[HO–Co–CH_3]^+$.

Schröder *et al.* report that reacting Fe^+ with *acetic acid* produces $[HO–Fe–CH_3]^+$ and $[H_2O–Fe=CH_2]^+$ in a 1:4 ratio in their CA studies. We find a similar result for Fe^+ and Co^+ in our laser ablation source, although the ratio of the intermediates depends on the acetic acid concentration and source conditions. The $[H_2O–M=CH_2]^+$ intermediate is readily identified, as it primarily photodissociates to form $MCH_2^+ + H_2O$. Schröder *et al.* report that reacting *n-propanol* with Fe^+ produces $[HO–Fe–CH_3]^+$ and $[H_2O–Fe=CH_2]^+$ in 10:1 ratio. We also observe these two intermediates from reaction of laser-ablated Fe^+ and Co^+ with

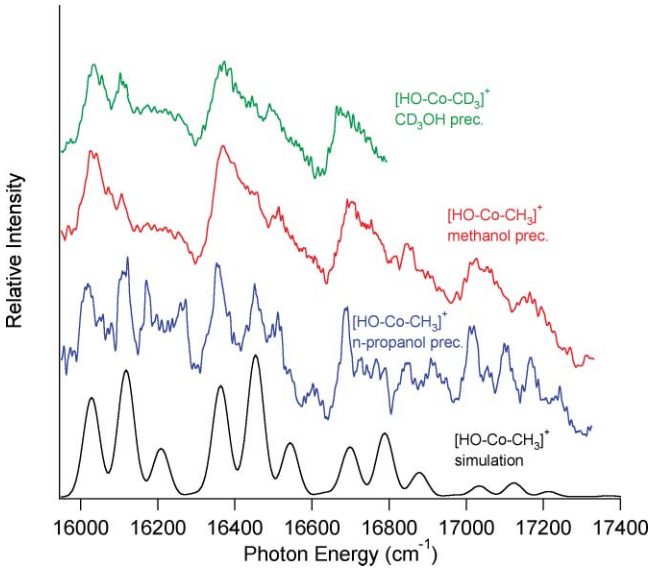

FIG. 3. Electronic photodissociation spectra of insertion intermediate. The top two traces show $[HO–Co–CH_3]^+$ and $[HO–Co–CD_3]^+$ produced via reaction of Co^+ with CH_3OH and CD_3OH. These spectra show a progression in the Co–C stretch, at 355 and 320 cm^{-1}, respectively. The third trace shows the spectrum of $[HO–Co–CH_3]^+$ obtained via reaction with n-propanol. This spectrum is more clearly resolved and also clearly shows a progression in the O–Co–C bend, at 90 cm^{-1}. The bottom trace is a simulated spectrum.

n-propanol. Reaction of laser-ablated Co^+ with n-propanol produces relatively more $[HO–Co–CH_3]^+$ (and less $[H_2O–Co{=}CH_2]^+$) than reaction with acetic acid, based on our spectroscopic results, shown below.

An additional potential complication in studies of transition metal reaction intermediates is the possible presence of low- and high-spin states at similar energies. This is particularly problematic for the $FeO^+ + CH_4 \rightarrow Fe^+ + CH_3OH$ system, in which the minimum energy pathway goes from high-spin reactants to low-spin intermediates, and back to high-spin products. However, this is less of an issue for $CoO^+ + CH_4 \rightarrow Co^+ + CH_3OH$. Although the ground state of CoO^+ is a quintet, Co^+ has a triplet ground state and low-spin triplet states are calculated to be significantly more energetically favorable for the intermediates. As a result, reaction of Co^+ with organic precursors produces triplet intermediates.

C. Electronic spectroscopy of $[HO–Co–CH_3]^+$

The electronic photodissociation spectra of $[HO–Co–CH_3]^+$ produced by reacting laser ablated Co^+ with methanol and n-propanol are shown in Figure 3. In each case, the only fragment observed is Co^+. This result is quite different from what we measure in photodissociation of $[HO–Fe–CH_3]^+$ and $Fe^+(CH_3OH)$ near 300 nm, where, for both intermediates, Fe^+ *and* $FeOH^+$ are observed, with similar intensities. The photodissociation results parallel the products observed for the thermal $MO^+ + CH_4$ reaction and differences between $[HO–Co–CH_3]^+$ and $[HO–Fe–CH_3]^+$ are likely due to the different thermodynamics of the two systems. The Fe^+–OH bond strength is significantly higher than that of Co^+–OH (366 vs 300 kJ/mol).[40] As a result, $Fe^+ + CH_3OH$ lies only 14 kJ/mol below $FeOH^+ + CH_3$, while $Co^+ + CH_3OH$ is 80 kJ/mol below $CoOH^+ + CH_3$.

Using acetic acid as a precursor, two products are observed, Co^+ and $CoCH_2^+$. The spectrum obtained using acetic acid precursor and monitoring Co^+ is nearly identical to that obtained with methanol, and is not shown. The major fragment observed is $CoCH_2^+$ (loss of H_2O), which is characteristic of $[H_2O–Co{=}CH_2]^+$. The photodissociation spectrum obtained by monitoring $CoCH_2^+$ is broad. This is similar to what we previously observed with $[H_2O–Fe{=}CH_2]^+$, where photolysis of the aquo-carbene intermediate provides an indirect means to measure the photodissociation spectrum of MCH_2^+ at energies below $D_0(M^+–CH_2)$, although the presence of the H_2O shifts the electronic spectrum.[23] We have previously measured the photodissociation spectrum of $CoCH_2^+$ directly, in the UV.[38] It shows an onset at 360 nm, with broad vibrational structure from 310 to 320 nm.

The electronic photodissociation spectrum of $[HO–Co–CH_3]^+$ produced via reaction with methanol (Figure 3, red trace) shows a series of broad peaks spaced by 335 cm^{-1}, with partially resolved peaks at smaller spacing. The spectrum obtained using n-propanol is more clearly resolved, with progressions in two vibrations in the excited state, at 335 cm^{-1} and 90 cm^{-1}. The peaks are superimposed on a very broad photodissociation peak that continues further to the red. However, no additional vibrational structure is observed. We observe similar spectra with all three precursors. As discussed above, reaction of Fe^+ with acetic acid and n-propanol has been shown to produce the insertion intermediate and not the exit channel complex. Thus, it is most likely that the $[HO–Co–CH_3]^+$ insertion intermediate is responsible for the structure in the spectrum, although $Co^+(CH_3OH)$ may contribute to the broad, nonresonant dissociation. The relative photodissociation yield is different for the three precursors, with n-propanol giving the highest dissociation yield, implying that reaction of Co^+ with n-propanol gives relatively more $[HO–Co–CH_3]^+$ than the other precursors. Ions produced via reaction with n-propanol clearly give the sharpest spectrum. This likely reflects differences in the vibrational temperature of $[HO–Co–CH_3]^+$ from different precursors. Reaction of Co^+ with methanol to produce $[HO–Co–CH_3]^+$ is calculated to be 83 kJ/mol exothermic (Fig. 1). Thus, the initially formed ions are highly vibrationally excited, and many collisions with the helium buffer gas are required to cool them. Vibrational hot- and sequence-bands thus contribute to the breadth in the methanol spectrum. In contrast, the reaction of Co^+ with n-propanol to produce $[HO–Co–CH_3]^+ + C_2H_4$ is calculated to be ~21 kJ/mol endothermic. As a result, the $[HO–Co–CH_3]^+$ formed is likely to be vibrationally colder, especially considering that the C_2H_4 product can also take away energy.

We also react Co^+ with CD_3OH in He to produce $[HO–Co–CD_3]^+$. The resulting spectrum is shown in green in Figure 3. The major progression shows a modest isotopic shift, from 335 cm^{-1} to 320 cm^{-1}. The electronic photodissociation spectrum of $[HO–Co–CH_3]^+$ is similar to that of $[HO–Fe–CH_3]^+$ measured by Aguirre *et al.*[23] In $[HO–Fe–CH_3]^+$, there is an extensive progression in the Fe–C stretch (478 cm^{-1}) and shorter progressions in the Fe–O stretch (861 cm^{-1}) and O–Fe–C bend (132 cm^{-1}). We assign the

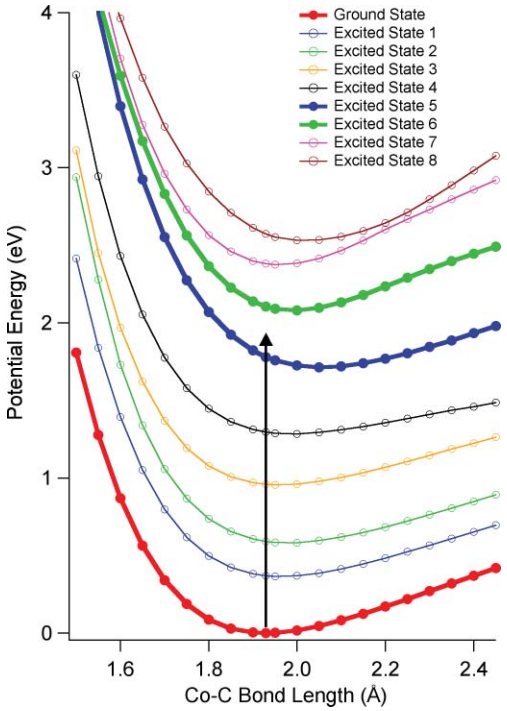

FIG. 4. Calculated ground and excited electronic states of $[HO–Co–CH_3]^+$, showing the potential along the Co–C stretch coordinate. The TDDFT calculations are at the B3LYP/6-311+G(*d*,*p*) level. Electronic excitation generally leads to a longer Co–C bond. The electronic state observed in the experiments near 16 000 cm^{-1} corresponds to excited state 5.

335 cm^{-1} vibration in $[HO–Co–CH_3]^+$ to the Co–C stretch and the 90 cm^{-1} vibration to the O–Co–C bend. This assignment is supported by time-dependent DFT (TD-DFT) calculations of the excited state Co–C stretching potential (see below). The excited state M–C stretching and O–M–C bending frequencies are lower for the Co complex than for the Fe complex. The ratios of the M–C stretching frequency for the two isotopes $\rho = \nu_{[HOM-CD_3]^+}/\nu_{[HOM-CH_3]^+}$ are similar for the two metals: 0.955 for Co and 0.969 for Fe. The vibrational structure in $[HO–Fe–CH_3]^+$ is slightly sharper, presumably because the excited electronic state is longer-lived. A Franck-Condon analysis of the electronic spectrum was carried out in order to estimate the geometry change upon electronic excitation. The ground state Co–C stretching and bending frequencies were set to the B3LYP/6-311+G(*d*,*p*) values (424 and 163 cm^{-1}, respectively), and the vibrations were assumed to be harmonic and separable. The best-fit simulation is shown in black in Figure 3. It corresponds to a displacement of 0.12 Å in the Co–C stretch and 8° in the O–Co–C bend. Similar displacements (0.13 Å and 4.4°) were observed[23] for $[HO–Fe–CH_3]^+$. The harmonic simulations do not indicate the direction of the displacement. However, electronic excitation likely leads to lengthening of the Co–C bond because the Co–C stretching frequency is significantly lower in the excited state than in the ground state. This is supported by TD-DFT calculations.

In order to further characterize the triplet excited electronic states of $[HO–Co–CH_3]^+$ we carried out TD-DFT calculations at the B3LYP/6-311+G(*d*,*p*) level. Figure 4 shows a scan along the Co–C bond, with all other coordinates fixed at the equilibrium ground state value. Excited state 5, shown in blue, is in excellent agreement with the observed electronic spectrum. It has an equilibrium Co–C bond length of 2.057 Å. This corresponds to a calculated displacement of 0.127 Å, in excellent accord with experiment. By numerically solving the Schrodinger equation on the calculated excited state potential, we calculate the Co–C stretching frequency to be 376 cm^{-1}, slightly higher than is observed. The calculated term value is 13 800 cm^{-1}, in decent agreement with the observed T_0 = 16 020 cm^{-1}. The next excited state, shown in green, better matches the observed transition energy (calculated T_0 = 16 800 cm^{-1}), but is a poorer match to the excited state frequency (478 cm^{-1}) and displacement (0.062 Å). Scanning the bend potential, excited state 5 is calculated to have an O–Co–C angle of 117.5°, which is 13° larger than the ground state, in accord with experiment.

D. Vibrational spectroscopy of reaction intermediates

Vibrational spectra of two reaction intermediates – $[HO–Co–CH_3]^+$ and $[H_2O–Co{=}CH_2]^+$, with potential contributions from $Co^+(CH_3OH)$ – were measured using photofragment spectroscopy. In order to obtain vibrational spectra using photofragment spectroscopy, absorption of a photon needs to lead to bond breaking. One photon in the O–H stretching region only has ~43 kJ/mol of energy, so photodissociation of the intermediates requires at least two to five photons, depending on the intermediate. Vibrational spectra were thus measured using IRMPD and by IR-REPD of argon-tagged molecules $[CoCH_4O]^+(Ar)$. Our study of intermediates of the $FeO^+ + CH_4$ reaction also used these techniques.[24]

In IRMPD, the molecule sequentially absorbs several photons, which provide the energy required to break the weakest bond. Also, the energy needs to flow from the vibration excited to the dissociation coordinate. The efficiency of IRMPD is enhanced by a high density of vibrational states and rapid intramolecular vibrational redistribution (IVR) which maintains the resonance that would otherwise be lost due to anharmonicity and transfers energy from the vibration excited to the dissociation coordinate.[41] Small molecules such as $[HO–Co–CH_3]^+$ have relatively high binding energies and low IVR rates, and thus are challenging to study using IRMPD. The efficiency of IRMPD strongly depends on the laser fluence and, in this study, is greatly improved by multi-passing the IR beam. Unfortunately, spectra measured by IRMPD tend to be broad. This is due to saturation caused by the high laser powers used as well as to preferential photodissociation of vibrationally excited molecules, which require fewer photons to dissociate.[24] These problems can be overcome by measuring vibrational spectra of ions bound to a rare gas atom such as argon ("argon-tagging").[42–44] The tag is sufficiently weakly bound that absorption of one IR photon by the chromophore leads to loss of the tag. Using a weakly bound tag usually ensures that perturbations to the spectrum are small. However, there are some ions for which rare-gas tagging significantly perturbs the spectrum.[44,45] We measure, and use calculations to predict, spectra with and without argon atoms. Vibrational resonances observed via tagging are

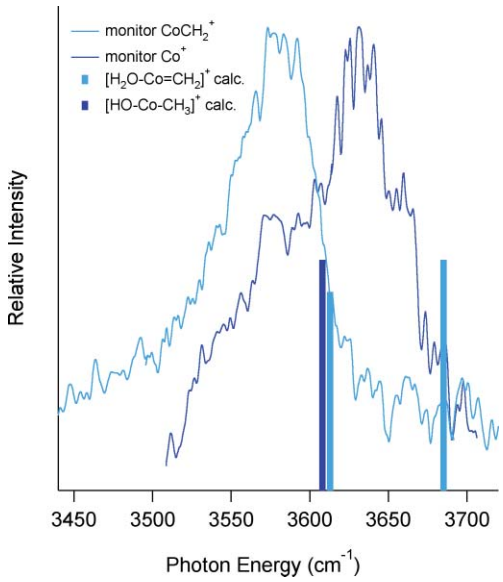

FIG. 5. Vibrational spectra of $[CoCH_4O]^+$ ions produced by reacting Co^+ with acetic acid. Spectra are obtained by IRMPD. Two intermediates are formed, with distinctive spectra and dissociation pathways. IRMPD of $[H_2O–Co=CH_2]^+$ produces $CoCH_2^+$, while $[HO–Co–CH_3]^+$ dissociates to form Co^+. The spectrum monitoring Co^+ has been multiplied by factor of 10. Vertical bars indicate vibrational frequencies and relative intensities calculated at the B3LYP/6-311+G(*d*,*p*) level and scaled by 0.961.

usually sharp. This is due to the one-photon dissociation, as well as to the small ion-Ar binding energies, which ensure that Ar-tagged ions are vibrationally cold.

1. IRMPD spectra

In a series of experiments, $[CoCH_4O]^+$ ions are produced by reacting laser-ablated Co^+ with methanol, acetic acid, and n-propanol, and the vibrational spectra of the resulting ions measured using IRMPD. Different precursors can produce different intermediates. The intermediates often differ in their dissociation pathways and vibrational spectra. The electronic photodissociation shows that reaction of Co^+ with acetic acid produces $[H_2O–Co=CH_2]^+$ (which photodissociates to $CoCH_2^+$) and $[HO–Co–CH_3]^+$ (which photodissociates to Co^+). In IRMPD, we observe the same products. Figure 5 shows IR photodissociation spectra obtained by monitoring Co^+ and $CoCH_2^+$. The two spectra are clearly different, indicating that they are due to two different intermediates.

The photodissociation spectrum obtained by monitoring $CoCH_2^+$ (Fig. 5, light blue) consists of a peak at 3580 cm^{-1} with FWHM of ~70 cm^{-1}. The $CoCH_2^+$ fragment is characteristic of the $[H_2O–Co=CH_2]^+$ intermediate. This intermediate is calculated to have two stretches in this region, due to the symmetric and antisymmetric O–H stretches in H_2O at 3613 and 3685 cm^{-1}, respectively (light blue bars). In the IRMPD spectrum we only observe the symmetric stretch vibration. The calculations predict similar absorption intensities for the two vibrations, as shown in Table II. Our inability to observe the antisymmetric stretch vibration is thus likely due to inefficient dissociation. IRMPD requires efficient IVR, to quickly transfer energy from the initially excited vibration to other vibrations in the molecule, and, eventually, to the dissociation coordinate. It is likely that IVR is inefficient for the antisymmetric stretch as there are few other vibrations with b_2 symmetry and it is the highest frequency vibration in the molecule. Dissociation efficiencies that vary dramatically for different vibrations have been previously observed in IRMPD studies.[46] Binding to $CoCH_2^+$ is calculated to redshift the symmetric and antisymmetric O–H stretches in water by 55 and 83 cm^{-1}, respectively. We observe a slightly larger shift, 77 cm^{-1}, for the symmetric stretch. We have also measured O–H stretching frequencies in $Co^+(H_2O)$ using vibrationally mediated photodissociation.[47] It exhibits similar redshifts: the O–H stretching frequencies are 3612 and 3692 cm^{-1}. Several other metal cation-H_2O complexes show similar redshifts in the O–H stretches.[43,48] The shift is thought to be due to the cation removing electron density from the oxygen, thereby slightly weakening the O–H bonds.

The photodissociation spectrum obtained by monitoring Co^+ peaks at 3630 cm^{-1}. This spectrum is somewhat

TABLE II. Harmonic vibrational frequencies for bare and argon-tagged $CoO^+ + CH_4$ reaction intermediates at the B3LYP/6-311+G(*d*,*p*) level. IR intensities (km/mol) in parentheses. Frequencies are scaled by 0.961.

	O–H stretch (cm^{-1})	C–H stretches (cm^{-1})
CH_3OH	3697(30)	2992(27), 2919(64), 2873(68)
$[HO–Co–CH_3]^+$ triplet	3608(240)	3079(12), 2991(3), 2834(36)
$[HO-Co-CH_3]^+$ quintet	3636(508)	3021(9), 3006(10), 2882(49)
$[HO-Co-CH_3]^+$(Ar) triplet	3629(228)	3084(5), 3006(2), 2889(23)
$[HO-Co-CH_3]^+$(Ar) quintet	3634(424)	3019(5), 3017(7), 2891(38)
$Co^+(CH_3OH)$ triplet	3649(154)	3054(2), 3042(1), 2948(7)
$Co^+(CH_3OH)$ quintet	3604(137)	3051(1), 3049(0.2), 2950(2)
$Co^+(CH_3OH)$(Ar) triplet	3654(154)	3054(3), 3040(2), 2947(8)
$Co^+(CH_3OH)$(Ar) quintet	3605(138)	3053(1), 3046(0.5), 2950(3)
H_2O	3768(57), 3668(10)	...
$[H_2O–Co=CH_2]^+$ triplet	3685(247), 3613(213)	3021(0.5), 2942(5)
$[H_2O–Co=CH_2]^+$ quintet	3672(261), 3600(211)	3081(10), 2958(19)
$[H_2O–Co=CH_2]^+$(Ar) triplet	3690(236), 3616(196)	3024(0.2), 2945(5)

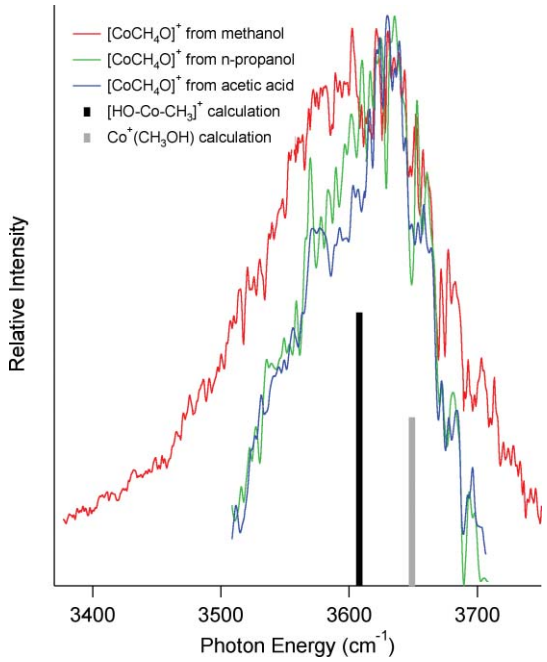

FIG. 6. Vibrational spectra of $[CoCH_4O]^+$ produced by reacting Co^+ with different precursors. Spectra are obtained by IRMPD, monitoring the Co^+ fragment, and are scaled to have the same maximum intensity. Vertical bars indicate vibrational frequencies and relative intensities calculated at the B3LYP/6-311+G(*d*,*p*) level and scaled by 0.961.

noisy, as the maximum Co^+ yield is only 10% of the maximum $CoCH_2^+$ yield. The electronic spectroscopy confirms that reaction of laser-ablated Co^+ with acetic acid produces $[H_2O–Co=CH_2]^+$ and $[HO–Co–CH_3]^+$. We thus assign the peak at 3630 cm^{-1} to the O–H stretch of the $[HO–Co–CH_3]^+$ insertion intermediate. Initially, it is surprising that IRMPD of $[HO–Co–CH_3]^+$ does not produce $CoOH^+$, as this dissociation pathway requires simply breaking a bond, while production of $Co^+ + CH_3OH$ involves substantial rearrangement. However, as Figure 1 shows, $CoOH^+ + CH_3$ is energetically unfavorable, as it lies 88 kJ/mol above TS2, and 93 kJ/mol above $Co^+ + CH_3OH$. The two pathways are much closer in energy for the corresponding iron system, and IRMPD of $[HO–Fe–CH_3]^+$ produces Fe^+ and $FeOH^+$.[24]

We used two other precursors, n-propanol and methanol, to prepare $[CoCH_4O]^+$. Using n-propanol also produces $[H_2O–Co=CH_2]^+$ and $[HO–Co–CH_3]^+$, but the relative amounts are very different than is observed with acetic acid. The Co^+ fragment dominates, indicating higher yield of $[HO–Co–CH_3]^+$. The IRMPD spectrum obtained by monitoring $CoCH_2^+$ is similar to that shown for acetic acid in Figure 5. Figure 6 compares vibrational spectra measured by monitoring the Co^+ fragment from IRMPD of $[CoCH_4O]^+$ formed from the three precursors. Spectra from acetic acid and n-propanol precursors are very similar, consisting of a slightly asymmetrical peak at 3630 cm^{-1}, with 100 cm^{-1} FWHM. Using methanol as a precursor, Co^+ is the only fragment observed. The resulting spectrum is broader, particularly to the red. The broadening is likely due to preferential photodissociation of vibrationally hot molecules produced in the source, as well as to overlapping spectra due to the insertion and $Co^+(CH_3OH)$ exit channel intermediates. Our observed ν_{OH} in $[HO–Co–CH_3]^+$ is very similar to the measured value[24] in $[HO–Fe–CH_3]^+$, 3623 cm^{-1}. The B3LYP calculations predict $\nu_{OH} = 3608$ cm^{-1} in $[HO–Co–CH_3]^+$, which is close to our observed value, 3630 cm^{-1}. The calculations slightly underestimate ν_{OH} for $[HO–Co–CH_3]^+$ and slightly overestimate ν_{OH} for $[H_2O–Co=CH_2]^+$. Both values are consistent with the 33 cm^{-1} RMS error reported in a systematic study of B3LYP/6-311+G(*d*,*p*) frequencies for a series of molecules, using a scaling factor of 0.961.[30]

2. Vibrational spectroscopy: Argon-tagged insertion intermediate

Photodissociation spectra obtained by IRMPD tend to emphasize contributions from vibrationally excited ions, which lead to broadening, especially to lower photon energy. Spectra obtained from argon-tagged molecules thus tend to be narrower. Argon-tagged $[HO–Co–CH_3]^+$ is produced using the same precursors as for the IRMPD experiments, using argon as the carrier gas.

Argon binding energies have not been measured for these molecules. However, argon binds very strongly to bare Co^+ ($D_0 = 4111 \pm 5$ cm^{-1}).[49] Our B3LYP/6-311+G(*d*,*p*) calculations predict that argon binds fairly strongly to triplet $[HO–Co–CH_3]^+$ ($D_0 = 2785$ cm^{-1}), weakly to $Co^+(CH_3OH)$ ($D_0 = 1138$ cm^{-1}) and even more weakly to $[H_2O–Co=CH_2]^+$ ($D_0 = 737$ cm^{-1}). Absorption of one photon in the O–H stretching region should readily lead to dissociation, and we observe much higher dissociation yields than for untagged molecules, with loss of argon the only dissociation pathway. Photodissociation spectra of $[HO–Co–CH_3]^+(Ar)$ produced using methanol, n-propanol, and acetic acid precursors are shown in Figure 7. Spectra obtained with the three precursors show the same O–H stretching frequency, 3642 cm^{-1}. The peaks in the Ar-tagged spectra are much

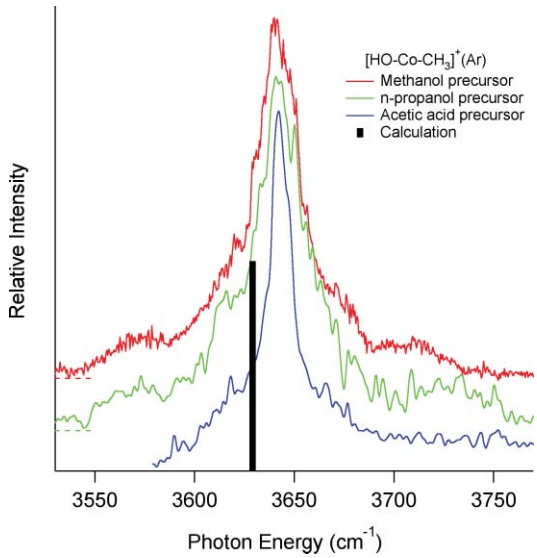

FIG. 7. Vibrational spectra of $[HO–Co–CH_3]^+(Ar)$ produced by reacting Co^+ with different precursors. Spectra are measured by monitoring argon loss. The vertical bar indicates the frequency calculated at the B3LYP/6-311+G(*d*,*p*) level and scaled by 0.961. The spectra are offset for clarity, and the dashed horizontal lines indicate the baseline for each spectrum.

sharper than in the IRMPD spectrum, with FWHM = 25 cm^{-1} (methanol and n-propanol) and 10 cm^{-1} (acetic acid) rather than 100 cm^{-1}. There is a small blueshift observed on Ar-tagging, of ~12 cm^{-1}, in accord with calculations (Table II), which predict a 21 cm^{-1} blueshift. The photodissociation spectra of $[HO–Co–CH_3]^+(Ar)$ and $[HO–Fe–CH_3]^+(Ar)$ are very similar, with ν_{OH} = 3647 cm^{-1} for the iron complex. Although IRMPD of $[H_2O–Co{=}CH_2]^+$ is observed near 3580 cm^{-1} (Fig. 5), we do not observe this peak in the Ar-tagged spectrum. This is likely due to the very low binding energy of argon to $[H_2O–Co{=}CH_2]^+$, which makes Ar-tagged complexes much more difficult to produce.

Combining our spectroscopic and computational results with previous studies of reaction kinetics and dynamics reveals several details of the mechanism of the $CoO^+ + CH_4$ reaction. Reaction studies at 300 K produce two striking results: the low efficiency of the reaction (0.5% of the collision rate), and the high selectivity for methanol production (100%).[10] The low reactivity at thermal energies is consistent with guided ion beam studies which find a reaction onset of 54 kJ/mol.[11] Our calculations predict that the barrier to produce the key $[HO–Co–CH_3]^+$ intermediate lies ~25 kJ/mol above reactants. The triplet and quintet barriers are calculated to be similar. This barrier leads to the low observed efficiency at low collision energies. This situation is very different from what is observed for the reactions of FeO^+ with methane and hydrogen, where the thermal reaction efficiency is determined by spin conversion from high-spin (sextet) reactants to low-spin (quartet) intermediates, as the quartet transition state lies well below the sextet.[50] The high selectivity for methanol production is due to the relative energies of TS2 (which leads to the $Co^+(CH_3OH)$ exit channel complex) and competing $CoOH^+ + CH_3$. Production of $CoOH^+ + CH_3$ is endothermic (Table I), while TS2 lies 77 kJ/mol below reactants. At higher collision energies, production of $CoOH^+$ is observed, and eventually dominates.[11] IRMPD of the $[HO–Co–CH_3]^+$ insertion intermediate only produces Co^+. The thermal $FeO^+ + CH_4$ reaction produces Fe^+ and $FeOH^+$ in a 41:57 ratio.[7] Again, formation of methyl radical (and metal hydroxide cation) dominates at higher collision energies.[9] IRMPD of $[HO–Fe–CH_3]^+$ produces Fe^+ and $FeOH^+$ in 45:55 ratio.[24] Thus, at least for these two systems, the half-reaction initiated by IRMPD of the insertion intermediate produces the same products as the thermal reaction, and with similar branching ratios.

IV. SUMMARY AND CONCLUSIONS

Electronic and vibrational spectra of intermediates of the gas-phase $CoO^+ + CH_4 \rightarrow Co^+ + CH_3OH$ reaction have been measured. Intermediates are produced via reaction of laser-ablated Co^+ with methanol, acetic acid, or n-propanol. The electronic spectrum of the triplet state of $[HO–Co–CH_3]^+$, the key insertion intermediate, shows vibrational progressions in the Co–C stretch (335 cm^{-1}) and O–Co–C bend (90 cm^{-1}). The vibrational spectra of $[HO–Co–CH_3]^+$ and $[H_2O–Co{=}CH_2]^+$ have been measured by IRMPD. Dissociation occurs via production of Co^+ and $CoCH_2^+$, respectively. For $[HO–Co–CH_3]^+$, ν_{OH} = 3630 cm^{-1}. Only the symmetric O–H stretch is observed for $[H_2O–Co{=}CH_2]^+$, at 3580 cm^{-1}. In addition, the vibrational spectra were measured via argon tagging, which results in much sharper vibrational resonances. For $[HO–Co–CH_3]^+(Ar)$, ν_{OH} = 3642 cm^{-1}. These frequencies are very similar to those observed in $[HO–Fe–CH_3]^+$ and $[HO–Fe–CH_3]^+(Ar)$.

An improved potential energy surface for the $CoO^+ + CH_4$ reaction is developed based on calculations at the CBS-QB3 level. Calculated energetics are in good agreement with those measured in guided ion beam studies.[11] The calculations predict that the reaction proceeds through the initial formation of a $OCo^+(CH_4)$ complex followed by isomerization over TS1 to the $[HO–Co–CH_3]^+$ insertion intermediate. The insertion intermediate can dissociate to produce $CoOH^+ + CH_3$ or isomerize via TS2 to the $Co^+(CH_3OH)$ exit channel complex, which then dissociates to $Co^+ + CH_3OH$. The barrier at TS1 lies 24 kJ/mol and 31 kJ/mol above the reactants for triplet and quintet states, respectively. This barrier explains the very low efficiency of this reaction at room temperature. However, once the insertion intermediate is formed, $Co^+ + CH_3OH$ is selectively produced, due to the low barrier at TS2, which lies 88 kJ/mol below $CoOH^+ + CH_3$. Initiating the "half-reaction" by photoexciting $[HO–Co–CH_3]^+$ either in the visible, or by multiple IR photons, exclusively produces Co^+, which parallels the results obtained in the thermal bimolecular reaction.[10]

ACKNOWLEDGMENTS

Financial support from the National Science Foundation (NSF) under Award No. CHE-0911225 is gratefully acknowledged.

[1] D. H. R. Barton, Aldrichim. Acta **23**, 3 (1990).
[2] M. H. Baik, M. Newcomb, R. A. Friesner, and S. J. Lippard, Chem. Rev. **103**, 2385 (2003); R. L. Lieberman and A. C. Rosenzweig, Nature (London) **434**, 177 (2005).
[3] K. Otsuka and Y. Wang, Appl. Catal., A **222**, 145 (2001); Y. Wang and K. Otsuka, J. Chem. Soc., Chem. Commun. **1994**, 2209 (1994).
[4] N. V. Beznis, B. M. Weckhuysen, and J. H. Bitter, Catal. Lett. **136**, 52 (2010); N. V. Beznis, A. N. C. van Laak, B. M. Weckhuysen, and J. H. Bitter, Microporous Mesoporous Mater. **138**, 176 (2011).
[5] R. A. Periana, D. J. Taube, S. Gamble, H. Taube, T. Satoh, and H. Fujii, Science **280**, 560 (1998).
[6] M. S. Chen and M. C. White, Science **318**, 783 (2007).
[7] D. Schröder and H. Schwarz, Angew. Chem., Int. Ed. Engl. **29**, 1433 (1990).
[8] M. F. Ryan, A. Fiedler, D. Schröder, and H. Schwarz, J. Am. Chem. Soc. **117**, 2033 (1995).
[9] D. Schröder, H. Schwarz, D. E. Clemmer, Y. Chen, P. B. Armentrout, V. Baranov, and D. K. Böhme, Int. J. Mass Spectrom. Ion Process. **161**, 175 (1997).
[10] M. F. Ryan, A. Fiedler, D. Schröder, and H. Schwarz, Organometallics **13**, 4072 (1994).
[11] Y.-M. Chen, D. E. Clemmer, and P. B. Armentrout, J. Am. Chem. Soc. **116**, 7815 (1994).
[12] D. Schröder and H. Schwarz, Angew. Chem., Int. Ed. Engl. **34**, 1973 (1995).
[13] A. Bozovic, S. Feil, G. K. Koyanagi, A. A. Viggiano, X. Zhang, M. Schlangen, H. Schwarz, and D. K. Bohme, Chem.-Eur. J. **16**, 11605 (2010).
[14] N. Dietl, C. van der Linde, M. Schlagen, M. K. Beyer, and H. Schwarz, Angew. Chem., Int. Ed. Engl. **50**, 4966 (2011).

[15]D. Schröder, H. Schwarz, and S. Shaik, Struct. Bonding (Berlin) **97**, 91 (2000); D. K. Böhme and H. Schwarz, Angew. Chem., Int. Ed. Engl. **44**, 2336 (2005); D. Schröder and H. Schwarz, Proc. Natl. Acad. Sci. U.S.A. **105**, 18114 (2008); J. Roithova and D. Schröder, Chem. Rev. **110**, 1170 (2010); H. Schwarz, "Chemistry with methane: Concepts rather than recipes," Angew. Chem., Int. Ed. Engl. (accepted).
[16]R. B. Metz, Int. Rev. Phys. Chem. **23**, 79 (2004); R. B. Metz, Adv. Chem. Phys. **138**, 331 (2008).
[17]Y. Shiota and K. Yoshizawa, J. Am. Chem. Soc. **122**, 12317 (2000).
[18]K. Yoshizawa, Y. Shiota, and T. Yamabe, J. Am. Chem. Soc. **120**, 564 (1998).
[19]J. Allison and D. P. Ridge, J. Am. Chem. Soc. **101**, 4998 (1979).
[20]A. M. L. Oiestad and E. Uggerud, Chem. Phys. **262**, 169 (2000).
[21]S. Hirabayashi, R. Okawa, M. Ichihashi, Y. Kawazoe, and T. Kondow, J. Chem. Phys. **130**, 164304 (2009).
[22]T. Shimanouchi, in *NIST Chemistry WebBook, NIST Standard Reference Database Number 69*, edited by P. J. Linstrom and W. G. Mallard (National Institute of Standards and Technology, Gaithersburg, MD, 1972).
[23]F. Aguirre, J. Husband, C. J. Thompson, K. L. Stringer, and R. B. Metz, J. Chem. Phys. **116**, 4071 (2002).
[24]G. Altinay, M. Citir, and R. B. Metz, J. Phys. Chem. A **114**, 5104 (2010).
[25]J. Husband, F. Aguirre, P. Ferguson, and R. B. Metz, J. Chem. Phys. **111**, 1433 (1999).
[26]D. Schröder, A. Fiedler, J. Hrusák, and H. Schwarz, J. Am. Chem. Soc. **114**, 1215 (1992).
[27]F. Aguirre, J. Husband, C. J. Thompson, K. L. Stringer, and R. B. Metz, J. Chem. Phys. **119**, 10194 (2003).
[28]D. Kaur, A. M. Desouza, J. Wanna, S. A. Hammad, L. Mercorelli, and D. S. Perry, Appl. Opt. **29**, 119 (1990).
[29]M. J. Frisch, G. W. Trucks, H. B. Schlegel, *et al.* GAUSSIAN 03, Gaussian, Inc., Pittsburgh, PA, 2004.
[30]M. P. Andersson and P. Uvdal, J. Phys. Chem. A **109**, 2937 (2005).
[31]J. A. Montgomery, M. J. Frisch, J. W. Ochterski, and G. A. Petersson, J. Chem. Phys. **110**, 2822 (1999); J. A. Montgomery, M. J. Frisch, J. W. Ochterski, and G. A. Petersson, J. Chem. Phys. **112**, 6532 (2000).
[32]C. E. Moore, in *NSRDS-NBS 35* (U.S. Government Printing Office, Washington, DC, 1949), vol. 2.
[33]M. N. Glukhovtsev, R. D. Bach, and C. J. Nagel, J. Phys. Chem. A **101**, 316 (1997).
[34]A. Irigoras, O. Elizalde, I. Silanes, J. E. Fowler, and J. M. Ugalde, J. Am. Chem. Soc. **122**, 114 (2000).
[35]M. N. Glukhovtsev, R. D. Bach, A. Pross, and L. Radom, Chem. Phys. Lett. **260**, 558 (1996).
[36]D. Feller and D. A. Dixon, J. Chem. Phys. **115**, 3484 (2001).
[37]A. Kamariotis, T. Hayes, D. Bellert, and P. J. Brucat, Chem. Phys. Lett. **316**, 60 (2000).
[38]J. Husband, F. Aguirre, C. J. Thompson, C. M. Laperle, and R. B. Metz, J. Phys. Chem. A **104**, 2020 (2000).
[39]M. Pavlov, M. R. A. Blomberg, P. E. M. Siegbahn, R. Wesendrup, C. Heinemann, and H. Schwarz, J. Phys. Chem. A **101**, 1567 (1997).
[40]P. B. Armentrout and B. L. Kickel, in *Organometallic Ion Chemistry*, edited by B. S. Freiser (Kluwer/Academic, Dordrecht, The Netherlands, 1994), pp. 1–46.
[41]J. Oomens, B. G. Sartakov, G. Meijer, and G. Von Helden, Int. J. Mass Spectrom. **254**, 1 (2006).
[42]M. Okumura, L. I. Yeh, J. D. Meyers, and Y. T. Lee, J. Chem. Phys. **85**, 2328 (1986); S. A. Corcelli, J. A. Kelley, J. C. Tully, and M. A. Johnson, J. Phys. Chem. A **106**, 4872 (2002); M. A. Duncan, Int. Rev. Phys. Chem. **22**, 407 (2003); A. Furuya, M. Tsuruta, F. Misaizu, K. Ohno, Y. Inokuchi, K. Judai, and N. Nishi, J. Phys. Chem. A **111**, 5995 (2007); K. R. Asmis, Mass Spectrom. Rev. **26**, 542 (2007).
[43]T. D. Vaden, J. M. Lisy, P. D. Carnegie, E. D. Pillai, and M. A. Duncan, Phys. Chem. Chem. Phys. **8**, 3078 (2006).
[44]O. Dopfer, Int. Rev. Phys. Chem. **22**, 437 (2003).
[45]N. I. Hammer, E. G. Diken, J. R. Roscioli, M. A. Johnson, E. M. Myshakin, K. D. Jordan, A. B. McCoy, X. Huang, J. M. Bowman, and S. Carter, J. Chem. Phys. **122**, 244301 (2005).
[46]L. MacAleese and P. Maitre, Mass Spectrom. Rev. **26**, 583 (2007).
[47]A. Kocak, G. Austein-Miller, G. Altinay, and R. B. Metz, "Electronic and vibrational spectroscopy of $Co^+(H_2O)$ and isotopomers" (to be submitted).
[48]R. S. Walters and M. A. Duncan, Aust. J. Chem. **57**, 1145 (2004); R. S. Walters, E. D. Pillai, and M. A. Duncan, J. Am. Chem. Soc. **127**, 16599 (2005); P. D. Carnegie, B. Bandyopadhyay, and M. A. Duncan, J. Phys. Chem. A **112**, 6237 (2008); P. D. Carnegie, A. B. McCoy, and M. A. Duncan, J. Phys. Chem. A **113**, 4849 (2009); P. D. Carnegie, B. Bandyopadhyay, and M. A. Duncan, J. Chem. Phys. **134**, 014302 (2011); T. D. Vaden, B. Forinash, and J. M. Lisy, J. Chem. Phys. **117**, 4628 (2002); A. L. Nicely, D. J. Miller, and J. M. Lisy, J. Mol. Spectrosc. **257**, 157 (2009).
[49]R. L. Asher, D. Bellert, T. Buthelezi, and P. J. Brucat, Chem. Phys. Lett. **227**, 277 (1994).
[50]D. Schröder, S. Shaik, and H. Schwarz, Acc. Chem. Res. **33**, 139 (2000); D. Danovich and S. Shaik, J. Am. Chem. Soc. **119**, 1773 (1997).